Journal of Power Sources 195 (2010) 146–150

Contents lists available at ScienceDirect

Journal of Power Sources

journal homepage: www.elsevier.com/locate/jpowsour

Short communication

Preparation and characterization of novel nickel–palladium electrodes supported by silicon microchannel plates for direct methanol fuel cells

Fengjuan Miao[a,b], Bairui Tao[a,b], Li Sun[a], Tao Liu[a], Jinchuan You[a], Lianwei Wang[a,*], Paul K. Chu[c]

[a] Key Laboratory of Polar Materials and Devices, Ministry of Education, and Department of Electronic Engineering, East China Normal University, Shanghai 200241, China
[b] College of Communications and Electronics Engineering, Qiqihar University, 42 Wenhua Street, Qiqihar Heilongjiang 161006, China
[c] Department of Physics and Material Sciences, City University of Hong Kong, Tat Chee Avenue, Kowloon, Hong Kong, China

ARTICLE INFO

Article history:
Received 22 May 2009
Received in revised form 2 July 2009
Accepted 3 July 2009
Available online 29 July 2009

Keywords:
Silicon microchannel plates
Methanol oxidation
Nickle–palladium catalyst
Integrated fuel cells

ABSTRACT

A novel anode structure based on the three-dimensional silicon microchannel plates (Si-MCP) is proposed for direct methanol fuel cells (DMFCs). Ni–Pd nanoparticles produced by electroless plating onto the Si-MCP inner sidewalls and followed by annealing at 300 °C under argon serve as the catalyst. In order to evaluate the electroactivity of the nanocomposites, Ni–Pd/silicon composites synthesized by the same method are compared. Scanning electron microscopy (SEM), energy-dispersive X-ray spectroscopy (EDS), and electrochemical methods are employed to investigate the Ni–Pd/Si-MCP anode materials. As a result of the synergetic effects rendered by the MCP and Ni–Pd nanoparticles, the Ni–Pd/Si-MCP nanocomposites exhibit superior electrocatalytic properties towards methanol electro-oxidation in alkaline solutions, as manifested by the negative onset potential and strong current response to methanol even during long-term cyclical oxidation of methanol. This new structure possesses unique and significant advantages such as low cost and integratability with silicon-based devices.

1. Introduction

Boating a high energy density and low pollution, fuel cells are the emerging alternative power sources for a myriad of applications in transportation, portable electronics, and residential power sources. Direct methanol fuel cells, known as DMFC, have been proposed for portable systems since methanol has a high intrinsic energy density. Thus, considerable attention and research work have been devoted to this area [1–3]. Despite substantial efforts and improvements so far, how to improve the catalyst utility and efficiency continues to hinder wider commercial viability of DMFCs, although significant progress has been made in acid DMFCs development [4,5]. Pt and the Pt-based nanoparticles are normally used as the catalyst because of the high electrocatalytic activity in methanol oxidation. In spite of the prospect, commercialization has been stifled by several issues. First of all, Pt and acid electrolyte membranes are quite expensive. Secondly, the cell performance diminishes because of serious activation polarization loss induced by the slow kinetics of the methanol oxidation reaction in acid media. Thirdly, the electrocatalyst suffers from corrosion in acid media. Hence, an alkaline medium is a promising alternative to enhance the performance of DMFCs and it has attracted increasing attention [6–10]. In alkaline DMFCs, relatively low cost metals such as Ag, Ni, Co [11,5] can be used as the electrode catalysts and OH^- ions in the electrolyte can provide faster kinetics in the oxygen reduction reaction.

It is an effective method to fabricate catalyst-supporting electrodes to disperse metal catalyst nanoparticles finely on the supporter so as to obtain a high surface to volume ratio in order to enhance the catalytic activity. Carbon-based backbones such as carbon nanotubes, carbon nanofibers, carbon nanocoils, and so on [12–17] have been proposed. In particular, 3D ordered mesoporous carbon (OMC) as support for metal nanocatalysts in electrode materials exhibits excellent performance in electro-oxidation of alcohol [18–20]. However, due to the incompatibility of carbon with microelectronics processing, it is difficult, or perhaps even unrealistic, to achieve monolithic integration of Si-based microfabricated fuel cells.

Here, we propose a MEMS-based direct methanol fuel cell. The backbone comprising 3D well-ordered Si-based MCP has many advantages, for instance, high surface to volume ratio, tunable pore size and channels depth, as well as interconnected pore network. More importantly, a new Pt-free catalyst can be synthesized by electroless plating of Ni–Pd onto the sidewall of a silicon microchannel plate (MCP) uniformly while at the same time using an alkaline electrolyte [21]. It has been demonstrated that the coated 3D electrode has better performance in electro-oxidation of methanol. The activity depends not only on the unique nature of the Ni–Pd nanoparticles, but also on the morphological structure of the Si MCP itself. The aim of this study is to not only overcome the cost problem of noble metal by using a new catalyst simple prepared by

* Corresponding author. Tel.: +86 21 54345160; fax: +86 21 54345119.
E-mail address: lwwang@ee.ecnu.edu.cn (L. Wang).

0378-7753/$ – see front matter © 2009 Elsevier B.V. All rights reserved.
doi:10.1016/j.jpowsour.2009.07.006

Ni–Pd electroless plating, but also meet the stringent demands by small-scale and portable applications.

2. Experimental details

Single side polished 100 mm ⟨1 0 0⟩ silicon wafers with a resistivity of 2–8 Ω cm and thickness of 525 μm were used as the starting materials to produce the silicon MCPs. Details of the preparation can be found elsewhere [22,23]. The Ni–Pd/Si-MCP nanocomposite structure was prepared by electroless plating. Before plating, the silicon MCP was laser cut into rectangular chips. After activation by dipping into Triton X-100 for 30 s, the sample was processed in a bath containing nickel and palladium source. The detailed procedures can be found in Ref. [24]. In order to accomplish better resistance ability in alkaline media, the Ni–Pd/Si-MCP nanocomposite was rapid thermal annealed for 400 s at 300 °C under argon to obtain nickel silicide layers [21]. Finally, a copper wire was glued onto the Ni–Pd/Si-MCP to form the electrical connection. The chips with an approximate area of about 0.25 cm^2 were encapsulated with silicone rubber to insulate the contacts from the electrolyte solution.

Scanning electron microscopy (SEM) and energy-dispersive X-ray spectroscopy (EDS) were employed to characterize the morphologies and components in the silicon MCP and Ni–Pd/Si-MCP electrode. Electrochemical investigations were carried out on a LK3200A electrochemical workstation (Tianjin, China). The Ni–Pd/Si-MCP nanocomposite electrode became the working electrode, a platinum wire electrode was used as the counter electrode, and a saturated calomel electrode (SCE) served as the reference electrode. The electrolyte was 2 M KOH and 2 M KOH/1 M CH_3OH. The potential was scanned between −0.6 and 0.2 V at a scanning rate of 50 mV s^{-1}. The experiments were conducted at room temperature (∼25 °C) and under 1 atm pressure.

3. Results and discussion

3.1. Morphologies

The surface morphologies of the silicon MCP and Ni–Pd/Si-MCP before and after electroless plating are characterized by SEM. The top view (Fig. 1(a)) and cross-sectional view (Fig. 1(b)) of the silicon MCP before electroless plating are presented. Fig. 2 exhibits the magnified picture of the top view (Fig. 2(a)) and the cross-sectional view (Fig. 2(b)) of the Ni–Pd/Si-MCP before electrochemical measurements. In order to study the influence of the electrochemical measurements, the corresponding picture of the cross-sectional SEM image after electrochemical measurement is depicted in Fig. 3. It can be clearly observed that the Si-MCP and Ni–Pd/Si-MCP have highly ordered microchannels with uniform diameters and lengths isolated and parallel to one another. Here, we choose the silicon MCP with a depth of about 150 μm and side length of each channel about 5 μm. After electroless plating, the inner sidewall of the silicon MCP is covered by a thin layer of Ni–Pd nanoparticals. The inner sidewall of the silicon MCP is coated homogeneously and the surface of the channels becomes rough. The sample microstructure and morphology before and after electrochemical measurement is more or less the same. Thus, it can be confirmed that Ni–Pd supported by the silicon MCP is stable in alkaline media.

The EDS results obtained from multiple areas, including all the areas of the top brim and the sidewalls in Fig. 4, show that the sidewalls of the MCPs mainly consist of Ni, Pd, as well as O, but no characteristic peaks of Si can be found, confirming the formation of a dense nickel layer. The major peaks correspond to Ni indicating little Pd agglomerate particles are coated onto the backbone of Ni/Si-MCP.

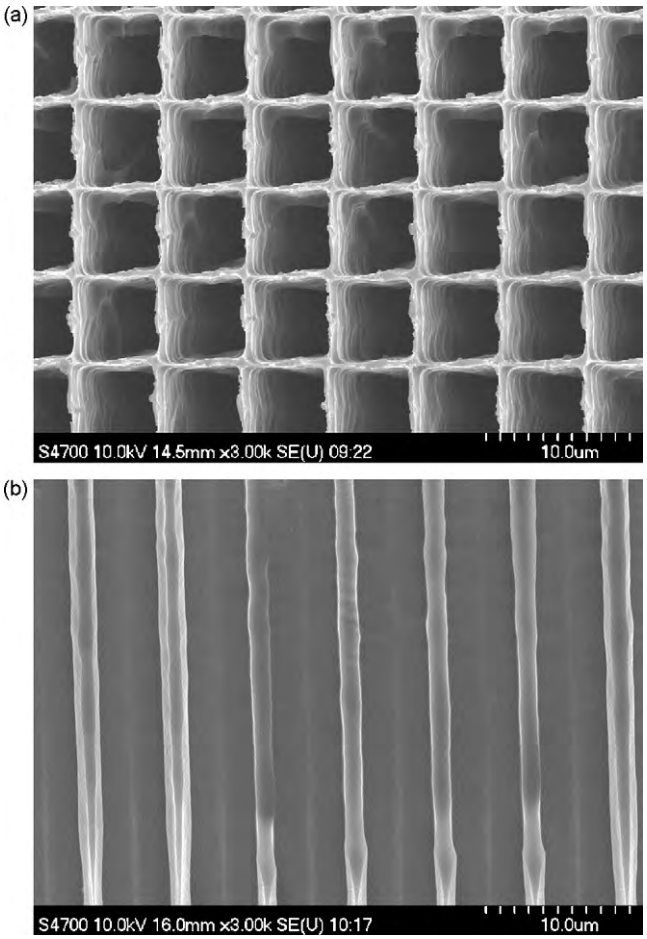

Fig. 1. (a) Top and (b) cross-sectional SEM images of the microstructure of the silicon MCP.

3.2. Electrocatalytic oxidation of methanol at the Ni–Pd/Si-MCP electrode

The electrocatalytic activity of the Ni–Pd/Si-MCP nanocompound is examined.

Fig. 5 shows the typical cyclic voltammograms (CVs) during methanol electro-oxidation on the Ni–Pd/Si-MCP (Fig. 5(a)) and Ni–Pd/Si (Fig. 5(b)) electrode in a 2 M KOH solution containing 1 M methanol using a scanning rate of 50 mV s^{-1}. The cyclic voltammograms of the Ni–Pd/Si-MCP and Ni–Pd/Si electrode in 2 M KOH in the absence of methanol is shown in the inset of Fig. 5, respectively.

In the CVs obtained in the 2 M KOH solution, the hump observed from the Ni–Pd/Si-MCP and Ni–Pd/Si electrode in the potential region from −0.2 to 0 V vs. SCE has a broad shoulder, and two reduction peaks exist at potentials −0.42 and 0 V, respectively. The current density of the Ni–Pd/Si-MCP is clearly greater then the Ni–Pd/Si.

Comparing to the CV in the absence of methanol in the potential range from −0.6 to 0.2 V, a methanol oxidation peak can be clearly observed on the two electrodes. The electro-oxidation of methanol is characterized by two well-defined current peaks in the forward and reverse scans. In the forward scan, the oxidation peak (A) corresponds to the oxidation of freshly chemisorbed species coming from methanol adsorption on the metal (M) catalysts it can be described as follows:

$$M + CH_3OH \leftrightarrow M\text{–}CH_3OH/_{ads} \quad (1)$$

$$M\text{–}CH_3OH/_{ads} + nOH^- \leftrightarrow \text{intermediates} + nH_2O + ne^- \quad (2)$$

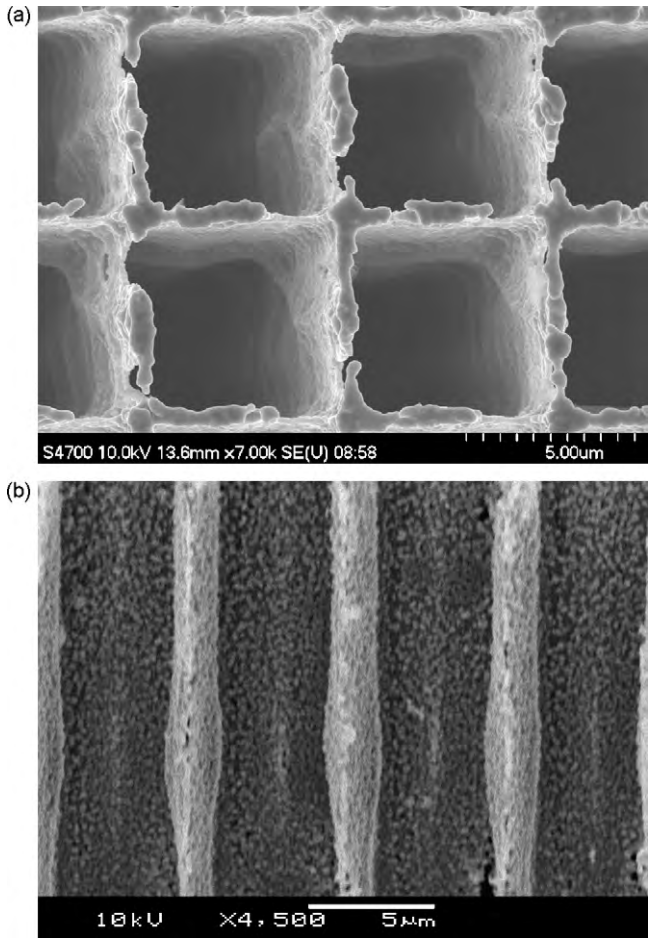

Fig. 2. (a) Top view and (b) magmified picture of the cross-sectional SEM images acquired from the microstructure of the Ni–Pd/silicon MCP before electrochemical measurements.

The deoxidize peak (B) is due to formation of Ni^{2+} hydroxide and Ni^{3+} oxy-hydroxide by the following mechanisms:

$$Ni + 2OH^- \rightarrow Ni^{2+} + 2e^-, \quad Ni^{2+} + OH^- \rightarrow Ni^{3+} + H_2O + e^- \quad (3)$$

The reoxidation peak (C) is primarily associated with the removal of incompletely oxidized carbonaceous species formed in

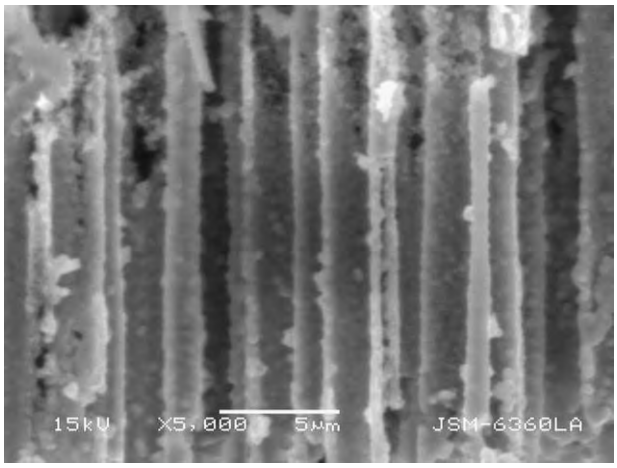

Fig. 3. Magnified pictures of the cross-sectional SEM images of the microstructure of the Ni–Pd/silicon MCP after electrochemical measurements.

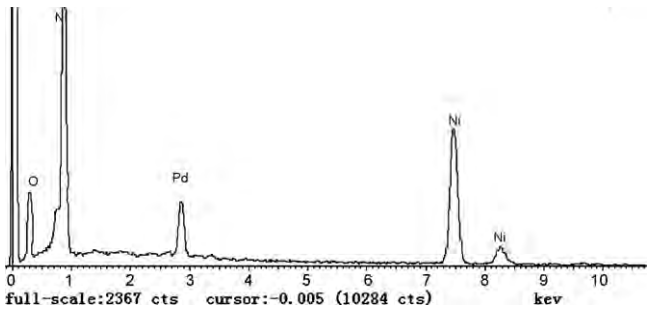

Fig. 4. Corresponding EDS image of the structure in Fig. 3.

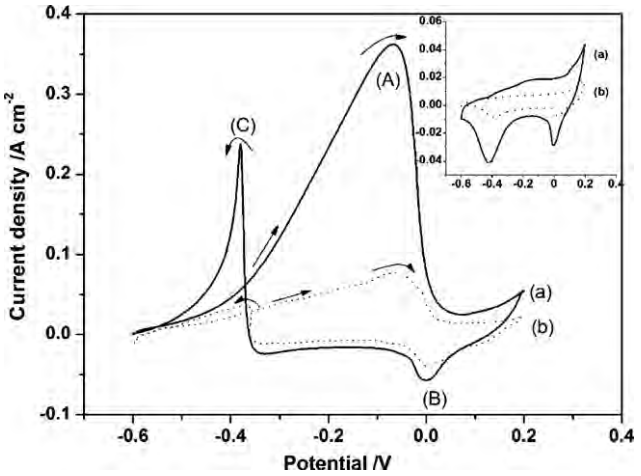

Fig. 5. Cyclic voltammograms of the Ni–Pd/Si-MCP (a) and Ni–Pd/Si (b) composite in 2.0 M KOH aqueous solution with and without methanol (in the inset) at room temperature with the scan rate of 50 mV s^{-1}.

the forward scan [25,26]:

$$M_2(CO)_{ads} + 3OH^- \rightarrow M\text{–}OH + M + CO_2 + H_2O + 3e^- \quad (4)$$

The electrochemical performances of the oxidation reaction of methanol on the Ni–Pd/Si-MCP and Ni–Pd/Si electrodes are given in Table 1. It can be observed that the current densities are higher at corresponding potentials on the Ni–Pd/Si-MCP electrode compared to those on the Ni–Pd/Si electrode. In the anode scan, the current density at −0.1 V for methanol oxidation on the Ni–Pd/Si-MCP electrode is about 6 times than that on the Ni–Pd/Si electrode. Furthermore, both electrodes show that the onset potential (*Es*) and peak potential (*E*p) for the oxidation of methanol are more negative, and the onset potential for methanol oxidation on the Ni–Pd/Si-MCP is 40 mV more negative than that of the Ni–Pd/Si electrode under the same conditions. The peak current of methanol oxidation on the Ni–Pd/Si-MCP electrode begins to rise much more sharply at a more negative potential, thereby directly improving the fuel cell efficiency. The negative onset potential indicates that the Ni–Pd nanoparticles on the ordered Si-MCP array can effectively reduce over potentials in the methanol electro-oxidation reaction. The magnitude of the peak current in the forward scan

Table 1
Electrochemical performance of the oxidation reaction of methanol on Ni–Pd/Si-MCP and Ni–Pd/Si electrodes.

Electrode	*Es* (V)	*E*p (V)	j_p (mA)	j_{at} (A) ($V = -0.1$)	*EASs* (cm^2)
Ni–Pd/Si-MCP	−0.55	−0.06	33.93	0.36	91.6
Ni–Pd/Si	−0.51	−0.05	3.28	0.06	30.4

Es: the onset potential; *E*p: peak potential (*E*p) for the oxidation of methanol at anodic scan; j_p: the current corresponding to *E*p; j_{at}: the current at −0.1 V.

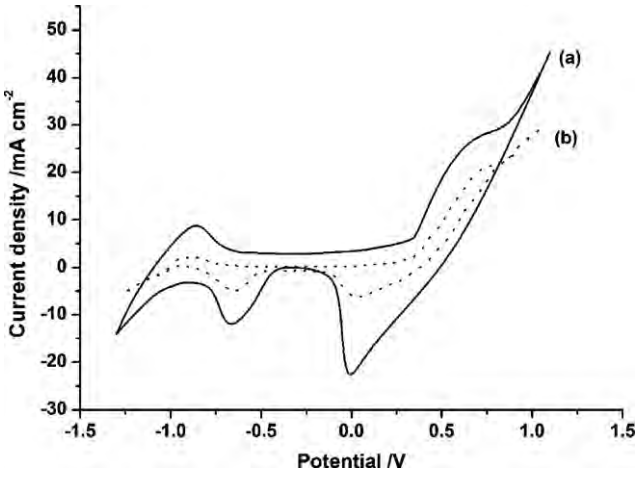

Fig. 6. Cyclic voltammograms of the Ni–Pd/Si-MCP (a) and Ni–Pd/Si (b) composite in 2.0 M KOH aqueous solution with broad potential range at the scan rate of 50 mV s^{-1}.

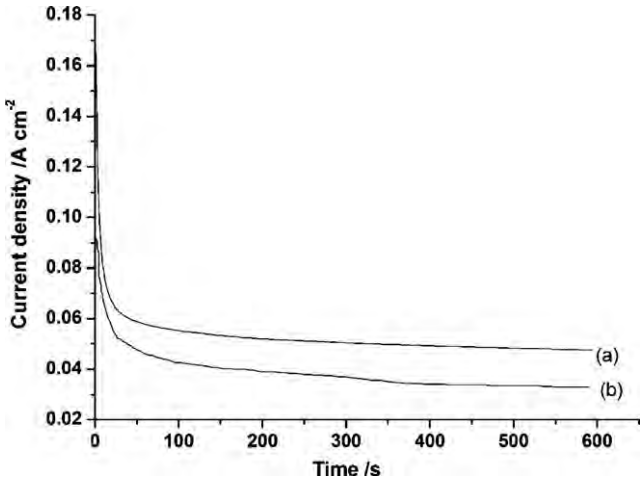

Fig. 7. Chronoamperogram of electroactivity of (a) Ni–Pd/Si-MCP and (b) Ni–Pd/Si electrode at an oxidation potential −0.4 V for methanol electro-oxidation in the 2 M KOH and 1 M methanol aqueous solution at 25 °C.

indicates better electrocatalytic activity of the electrocatalysts in the oxidation reaction of methanol in the alkaline medium. These results suggest that the Ni–Pd nanopaticles exhibit superior electrocatalytic activity towards methanol oxidation in an alkaline solution, and the Ni–Pd/Si-MCP has much higher catalytic activity for methanol electro-oxidation than Ni–Pd/Si in an alkaline medium.

Fig. 6 shows the cyclic voltammograms with broad potential range of the resulting Ni–Pd/Si-MCP and Ni–Pd/Si composite in 2 M KOH aqueous solution at the scan rate of 50 mV s^{-1}. It can be seen that the hydrogen adsorption/desorption peaks between −1.05 and −0.8 V is mainly due to the oxidation of the hydrogen absorbed on metal. The electrochemical active surfaces (*EASs*) of the catalysts can be determined by the charge consumed for hydrogen adsorption and the charge needed to reduce a monolayer of protons on metal catalysts [27].

It is obviously due to the larger electrochemical active surface area (*EASa*) consequently providing a larger surface to volume ratio for the support.

Because of the very large *ESAs*, the Ni–Pd/Si-MCP electrode has a better dispersion of metal nanoparticles compared to the Ni–Pd/Si electrode. This suggests that both the synergistic effect between Ni–Pd nanoparticles and structure effect of the Si-MCP enhance the catalytic activity of the Ni–Pd/Si-MCP nanocomposite in methanol oxidation. The 3D structure constitutes a proton conductive path from the catalysts to electrolyte membranes thereby playing an important role in the performance of the DMFCs. Besides the good electronic conductivity, the silicon MCP has well-ordered channels that bode well for facile molecular transport of the reactants and products enhancing molecular conversion [28]. The high volume to surface ratio increases the reaction area, and so more catalyst nanoparticles can be deposited onto the electrode surface resulting in the high surface reactivity. Our results demonstrate that this new catalyst supported by the silicon MCP electrode can significantly enhance the electrode kinetics.

The ratio of the forward anodic peak current (I_f) to the reverse anodic peak current (I_b) can be used to describe the catalyst tolerance to carbonaceous species accumulation [29]. A higher ratio of the forward anodic peak current density (I_f) to the reverse anodic peak current density (I_b) usually indicates better oxidation of methanol to CO_2 during the anodic scan. In our experiments, the ratios are estimated to be about 1.89 (after eliminated the background current) [30] for the Ni–Pd/Si-MCP electrode. Such a high value indicates the best CO resistance due to the effective dispersion of catalyst particles [31,32].

The chronoamperometric technique is an effective method to evaluate the electrocatalytic activity and stability of catalyst materials. Fig. 7 shows the chronoamperogram of the electroactivity of the Ni–Pd/Si-MCP (a) and Ni–Pd/Si (b) electrodes at an oxidation potential −0.4 V in methanol electro-oxidation in the 2 M KOH and 1 M methanol aqueous solution at 25 °C. As expected, the methanol oxidation current on the Ni–Pd/Si-MCP electrode is evidently higher than that on the Ni–Pd/Si. The chronoamperogram also shows that electrocatalytic oxidation of methanol is maintained at a high activity and is very stable during measurement for over 600 s. This observation implies that most CO species can be oxidized and removed from the Ni–Pd catalyst nanoparticles. All in all, our results indicate that the Ni–Pd/Si-MCP nanocoposite has the best electrocatalytic properties.

4. Conclusion

3D ordered Ni–Pd/Si-MCP thin film electrodes have been fabricated by combining conventional microelectronics technology with electrochemical techniques. According to the CV plots, the DMFCs composed of this electrode have excellent electrochemical activity to electro-oxidation of methanol, better tolerance to carbonaceous species accumulation, high reversibility, and best stability. These novel DMFCs are simple, inexpensive, easily integrated, and highly stable, and the technique can be readily applied to large-scale fabrication of Ni–Pd/Si-MCP electrodes in energy storage devices.

Acknowledgements

This work was supported by Shanghai Fundamental Key Project under contract number 08JC1408900. This work was also financially supported by the China NSFC support under the contract of Grant no. 50672027 and Hong Kong Research Grants Council (RGC) General Research Funds (GRF) no. CityU 112307.

References

[1] A.S. Arico, S. Srinivasan, V. Antonucci, Fuel Cells 1 (2001) 133.
[2] S.J. Shin, J.K. Lee, H.Y. Ha, S.A. Hong, H.S. Chun, I.H. Oh, J. Power Sources 106 (2002) 146.
[3] M. Hepel, I. Dela, T. Hepel, J. Luo, C.J. Zhong, Electrochim. Acta 52 (2007) 5529.
[4] W.J. Zhou, S.Q. Song, W.Z. Li, Z.H. Zhou, G.Q. Sun, Q. Xin, S. Douvartzides, P. Tsiakaras, J. Power Sources 140 (2005) 50–58.
[5] C. Coutanceau, L. Demarconnay, C. Lamy, J.-M. Léger, J. Power Sources 156 (2006) 14–19.

[6] K. Matsuoka, Y. Iriyama, T. Abe, M. Matsuoka, Z. Ogumi, J. Power Sources 150 (2005) 27–31.
[7] J. Bagchi, S.K. Bhattacharya, J. Power Sources 163 (2007) 661–670.
[8] P. Paul, J. Bagchi, S.K. Hattacharya, Indian J. Chem. Sect. A 45 (2006) 1144–1152.
[9] V. Rao, C. Hariyanto, U. Cremers, Stimming, Fuel Cells 7 (2007) 417–423.
[10] Z. Ogumi, K. Matsuoka, S. Chiba, M. Matsuoka, Y. Iriyama, T. Abe, M. Inaba, Electrochemistry 70 (2002) 980–983.
[11] K. Sawai, N. Suzuki, J. Electrochem. Soc. 151 (2004) A2132–A2137.
[12] E.S. Steigerwalt, G.A. Deluga, C.M. Lukehart, J. Phys. Chem. B 106 (2002) 760–766.
[13] T. Hyeon, S. Han, Y. Sung, K. Park, Y. Kim, Angew. Chem. Int. Ed. 42 (2003) 4352–4356.
[14] R. Yang, X. Qiu, H. Zhang, J. Li, W. Zhu, Z. Wang, X. Huang, L. Chen, Carbon 43 (2005) 11–16.
[15] C.A. Bessel, K. Laubernds, N.M. Rodriguez, R.T.K. Baker, J. Phys. Chem. B 105 (2001) 1115–1118.
[16] E.S. Steigerwalt, G.A. Deluga, D.E. Cliffel, C.M. Lukehart, J. Phys. Chem. B 105 (2001) 8079–8101.
[17] W. Li, C. Liang, W. Zhou, J. Qiu, H. Li, G. Sun, Q. Xin, Carbon 42 (2004) 436–439.
[18] R. Ryoo, S. Joo, H. Kruk, M. Jaroniec, Adv. Mater. 13 (2001) 677.
[19] J.S. Lee, S.H. Joo, R. Ryoo, J. Am. Chem. Soc. 124 (2002) 1156.
[20] M. Kruk, M. Jaroniec, T.W. Kim, R. Ryoo, Chem. Mater. 15 (2003) 2815.
[21] M. Bhaskaran, S. Sriram, L.W. Sim, J. Micromech. Microeng. (2008), 095002.
[22] X.M. Chen, J.L. Lin, D. Yuan, P.L. Ci, P.S. Xin, S.H. Xu, L.W. Wang, J. Micromech. Microeng. 18 (3) (2008) 037003.
[23] J.L. Lin, X.M. Chen, S.H. Xu, P.S. Xin, L.W. Wang, The 3rd IEEE International Conference on Nano/Micro Engineered and Molecular Systems, 2008, pp. 74–77.
[24] F.J. Miao, B.R. Tao, L. Sun, T. Liu, J.C. You, L.W. Wang, P.K. Chu, Sens. Actuat. B: Chem., doi:10.1016/j.snb.2009.05.002.
[25] M.C. Morin, C. Lamy, J.-M. Léger, J. Electroanal. Chem. 283 (1990) 287.
[26] J.C. Huang, Z.L. Liu, C.B. He, L.M. Gan, J. Phys. Chem. B 109 (2005) 16644.
[27] C.W. Xu, P.K. Shen, Chem. Commun. 19 (2004) 2238–2239.
[28] D.R. Rolison, Science 299 (2003) 1698.
[29] Y. Lin, X. Cui, C. Yen, C.M. Wai, J. Phys. Chem. B 109 (2005) 14410.
[30] P.L. Schilardi, R.C. Salvarezza, A.H. Creus, A.J. Arvia, S.L. Marvhino, J. Electroanal. Chem. 431 (1997) 81–98.
[31] M. Koudelka, J. Augustynski, J. Chem. Soc. Chem. Commun. 15 (1983) 855.
[32] B. Beden, F. Hahn, J.-M. Léger, C. Lamy, C.L. Perdriel, N.R. De Tacconi, R.O. Lezna, A.J. Arvia, J. Electroanal. Chem. 301 (1991) 129.